# Surface Characterization Study of the Thermal Decomposition of $Ag_2CO_3$

**William S. Epling and Gar B. Hoflund***

*Department of Chemical Engineering, University of Florida, Gainesville, Florida 32611*

**Ghaleb N. Salaita**

*Union Carbide Corporation, Technical Center, 3200 Kanawha Turnpike, South Charleston, West Virginia 25303*

*Received: November 1, 1997; In Final Form: January 27, 1998*

The changes in chemical states and composition of the surface region of a $Ag_2CO_3$ powder at various stages during thermal decomposition have been examined using X-ray photoelectron spectroscopy (XPS) and ion scattering spectroscopy (ISS). The near-surface region of the as-received powder consists primarily of $Ag_2CO_3$ although some hydrocarbon and alcohol contaminants also are present. A 155 °C anneal results in partial decomposition of $Ag_2CO_3$ to Ag metal and oxides and reduces the amounts of the C contaminants. An anneal at 170 °C causes further decomposition of the $Ag_2CO_3$ to Ag metal, $Ag_2O$, and AgO. ISS data indicate that at 205 °C oxygen migrates more rapidly to the outermost atomic layer than it desorbs, resulting in an increased oxygen concentration. The AgO species undergoes further decomposition to $Ag_2O$ during a 340 °C anneal treatment. Between 340 and 430 °C the $Ag_2O$ decomposes, leaving only Ag metal and subsurface oxygen in the near-surface region of the sample. These results are consistent with temperature-programmed reaction (TPR) data which exhibit a $CO_2$ peak at 260 °C and an $O_2$ peak at 420 °C. Both the XPS and TPR data indicate that the thermal decomposition of these species are activated since their decompositions occur at temperatures much higher than predicted by equilibrium thermodynamic calculations.

## Introduction

The oxygen−silver interaction has been studied extensively[1−18] due to the importance of this system in the silver-catalyzed epoxidation of ethylene to ethylene oxide.[19−30] Several forms of oxygen have been identified at Ag surfaces including atomic, molecular, and subsurface species as discussed in the review by Van Santen and Kuipers.[23] Studying the O−Ag interaction is complicated further by the presence of contamination which typically exists on air-exposed, as-prepared catalysts or model surfaces. Silver carbonate has been found to be a contaminant of air-exposed AgO and $Ag_2O$ powders[1,2] and is often present on air-exposed Ag metal surfaces. The surface chemistry of Ag is dependent on the sample history and surrounding environment. Furthermore, ethylene epoxidation catalysts are exposed to a recycle stream that contains $CO_2$ so $Ag_2CO_3$ probably exists at the catalyst surface during reaction. Therefore, studying the thermal behavior of $Ag_2CO_3$ is of interest.

Characterization studies of AgO and $Ag_2O$ samples[1,2] have shown that the complex processes and reactions that occur at varying temperatures can be examined by annealing the samples in a stepwise manner and characterizing the surface after each anneal. This procedure isolates the reactions that occur and allows for better understanding of the complex behavior and spectral features. X-ray photoelectron spectroscopy (XPS) was used to characterize the near-surface region of the oxide powders after each anneal, and then comparisons were made with spectra obtained before the anneal in order to examine the chemical changes that occur during the anneal. This not only provides an understanding of the thermal chemistry of the sample but also provides reference spectra from well-defined surfaces.[3−5]

The purpose of this investigation is to examine the thermal decomposition of $Ag_2CO_3$ to Ag oxides and then Ag metal with XPS, ion scattering spectroscopy (ISS), and temperature-programmed reaction (TPR). Using this approach, detailed spectral features have been obtained from $Ag_2CO_3$, and the steps in the thermal decomposition have been examined. Annealing temperatures were set at decomposition temperatures determined by monitoring the background pressure of the vacuum chamber and maintained for one-half hour. An increase in the background pressure indicates that thermal decomposition and gaseous desorption is occurring at a measurable rate.

## Experimental Section

The silver carbonate examined in this study was a high-purity powder (99.9%) purchased from AESAR. A second high-purity powder (99.999%) purchased from Aldrich was also studied, and excellent agreement with the results presented was obtained. The powder was pressed into pellet form in an Al cup and inserted into an UHV chamber (base pressure $< 10^{-10}$ Torr). Sample heating was accomplished radiatively using a tungsten filament located underneath the sample holder. The sample temperature was monitored using a K-type thermocouple positioned at the rim of the sample cup containing the $Ag_2CO_3$ powder.

XPS data were collected using a double-pass cylindrical mirror analyzer (DPCMA) (Perkin-Elmer PHI model 25-270AR) and a Mg Kα X-ray source. Data were collected by operating the CMA in the retarding mode using pass energies of 50 and 25 eV for survey spectra and high-resolution spectra, respectively. The sample was tilted 30° off the CMA axis. ISS spectra were collected while operating the CMA in the nonretarding mode using He ions generated by a PHI model 04-151 ion gun. An ion current of 33 nA over a 4 mm diameter spot and a scattering angle of 135° were used. Each spectrum was obtained in 66 s. These operating parameters result in a minimal

S1089-5647(98)00054-6 CCC: $15.00 
Published on Web 02/25/1998

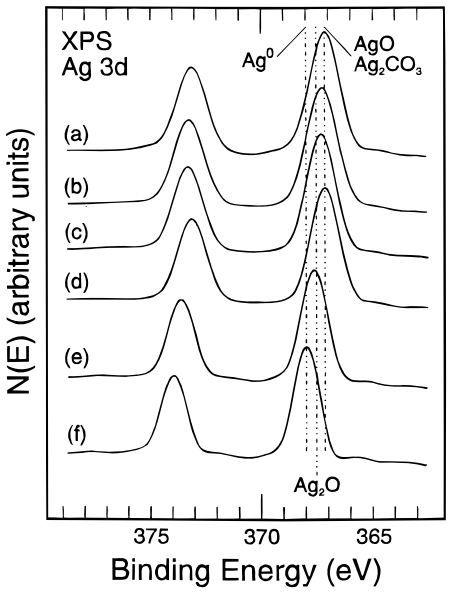


**Figure 1.** XPS Ag 3d spectra obtained from the as-received $Ag_2CO_3$ powder after (a) insertion into the UHV chamber, (b) a 155 °C anneal for $^1/_2$ h, (c) a 170 °C anneal for $^1/_2$ h, (d) a 205 °C anneal for $^1/_2$ h, (e) a 340 °C anneal for $^1/_2$ h, and (f) a 430 °C anneal for $^1/_2$ h.

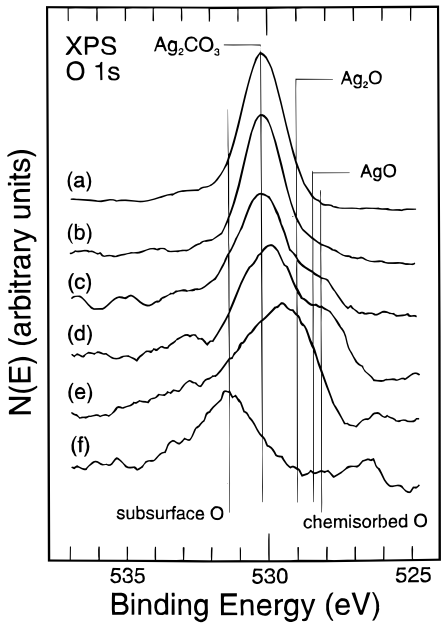


**Figure 2.** XPS O 1s spectra obtained from the as-received $Ag_2CO_3$ powder after (a) insertion into the UHV chamber, (b) a 155 °C anneal for $^1/_2$ h, (c) a 170 °C anneal for $^1/_2$ h, (d) a 205 °C anneal for $^1/_2$ h, (e) a 340 °C anneal for $^1/_2$ h, and (f) a 430 °C anneal for $^1/_2$ h.

amount of damage due to surface sputtering. Both XPS and ISS data were collected using pulse-counting detection.[31]

TPR data were obtained from $Ag_2CO_3$, AgO, and $Ag_2O$ using a mass-spectrometer-based instrument marketed by Altamira. These experiments were performed by placing 0.25 g of powder in a quartz tube and ramping the temperature from 20 to 550 °C at 10 °C/min under flowing He (30 $cm^3$/min). The gases monitored were $H_2$, $H_2O$, CO, $O_2$, and $CO_2$.

## Results and Discussion

An XPS survey spectrum obtained from the as-entered, $Ag_2CO_3$ sample (not shown) contains core-level and Auger features of Ag and O as well as a valence-band structure.[32] A small doublet due to the presence of a Pb impurity is also evident. This contaminant has also been observed at the surface of an as-prepared AgO sample.[1] Upon comparison of the survey spectrum shown in ref 32 to the spectra taken from AgO[1] and $Ag_2O$[2] samples, it is evident that the O 1s feature in the $Ag_2CO_3$ spectrum is larger with respect to the predominant Ag 3d peaks. This is expected since the stoichiometric ratio of O to Ag is 3:2 for $Ag_2CO_3$, which is larger than those at of AgO or $Ag_2O$.

The XPS Ag 3d features obtained from the as-entered silver carbonate sample are shown in Figure 1a. The Ag $3d_{5/2}$ peak has a binding energy (BE) of approximately 367.2 eV and a full width at half-maximum (fwhm) of 1.5 eV and is assigned as due to $Ag_2CO_3$. This value is in good agreement with that published by Hammond et al.[14] and near that reported by Weaver and Hoflund.[1] As depicted in Figure 1, Ag metal has a larger 3d BE that is atypical of the expected shift between a metal and its cation states. In most instances an initial state model is used in which only the core hole and nucleus interaction is considered. The screening of core-level electrons from the metal nucleus is reduced in the presence of the more electronegative anion such as oxygen. This diminished screening present in oxides increases the attraction of the unchanged nucleus to the core-level electrons, resulting in increased BEs of these electron. In the case of Ag, other factors beyond electronegativity differences strongly influence the BE positions of the Ag features. These may include the lattice potential, work function differences, and the extraatomic relaxation energy as discussed by Gaarenstroom and Winograd.[15]

An O 1s XPS spectrum taken from the as-entered $Ag_2CO_3$ sample is shown in Figure 2a. There is general agreement in the O/Ag literature regarding the XPS O 1s BEs of O in AgO, $Ag_2O$, and $Ag_2CO_3$ as discussed in detail in the previous parts of this study,[1,2] and lines corresponding to these assignments are shown in Figure 2. However, numerous other O species have been proposed, and the O 1s BE assignments vary considerably. Two other assignments have been made in this study. One is subsurface or oxygen atoms that are interstitially dissolved in the Ag metal lattice with an O 1s BE of 531.4 eV. There is a considerable amount of support for this assignment in the literature.[1,2] Another form is assigned as chemisorbed O with an O 1s BE of 528.3 eV. Although this assignment is consistent with the interpretation of the spectra presented in this and the previous parts of this study,[1,2] this assignment is tenuous. It is based on results obtained by Campbell and Paffett[33] and Campbell.[34] A large feature is centered at a BE of 530.2 eV, which corresponds to the O 1s BE value of $Ag_2CO_3$.[1,2,14,24] The O 1s peak is slightly asymmetric on the lower BE side. This is most likely caused by the presence of a small amount of $Ag_2O$ which has a BE of 528.8 eV.[3] A C 1s spectrum obtained from the as-entered $Ag_2CO_3$ powder is shown in Figure 3a. The primary carbon feature is due to carbonate species, and smaller contributions from alcohol and hydrocarbon contamination are also evident.[35] The accumulation of these contaminants is typical of air-exposed samples. The Ag(*MNN*) XPS spectrum taken from the as-entered $Ag_2CO_3$ powder is shown in Figure 4a. These features are more complex than XPS features because three electrons and many-body effects are involved in creating the Auger features. However, this often results in more significant changes in the shapes and positions of the Ag(*MNN*) peaks with varying Ag chemical state. The high-energy Ag(*MNN*) feature lies at a BE of 902.3 eV for $Ag_2CO_3$ in the XPS spectra. A small shoulder is also present due to Ag metal.

Quantification of the XPS data obtained from the as-entered $Ag_2CO_3$ sample was attempted using the homogeneous assump-

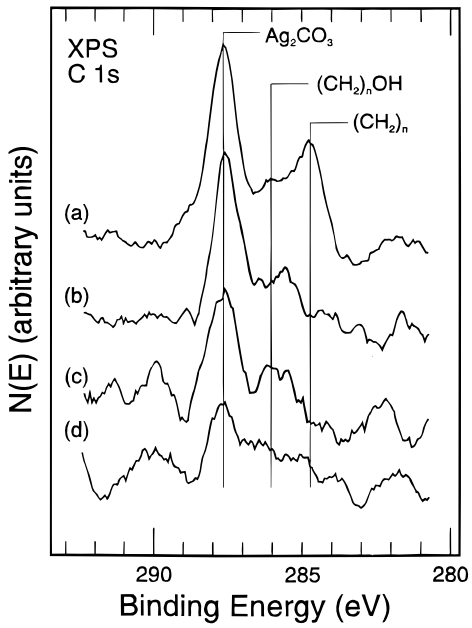


**Figure 3.** XPS C 1s spectra obtained from the as-received $Ag_2CO_3$ powder after (a) insertion into the UHV chamber, (b) a 155 °C anneal for $^1/_2$ h, (c) a 170 °C anneal for $^1/_2$ h, (d) a 205 °C anneal for $^1/_2$ h, (e) a 340 °C anneal for $^1/_2$ h, and (f) a 430 °C anneal for $^1/_2$ h.

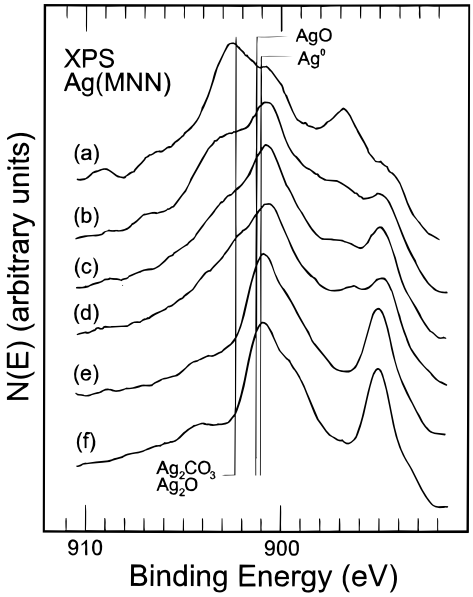


**Figure 4.** XPS Ag *MNN* spectrum obtained from the as-received $Ag_2CO_3$ powder after (a) insertion into the UHV chamber, (b) a 155 °C anneal for $^1/_2$ h, (c) a 170 °C anneal for $^1/_2$ h, (d) a 205 °C anneal for $^1/_2$ h, (e) a 340 °C anneal for $^1/_2$ h, and (f) a 430 °C anneal for $^1/_2$ h.

tion and the sensitivity factors listed in the first and second editions of the PHI handbook.[35,36] The very large difference between the earlier value of the sensitivity factor for Ag of 2.25 (ref 35) and the newer value of 5.987 (ref 36) suggests that neither of these values may be correct even though they apply to different types of analyzers. In this study the contributions of Ag metal and C species other than carbonates were subtracted from Ag 3d and C 1s peaks, respectively, and calculations were made to determine the near-surface compositions. Neither set of sensitivity factors yields acceptable compositions, so the C and Ag sensitivity factors were adjusted to give the $Ag_2CO_3$ composition. The different sensitivity factors and compositions obtained for this surface are shown in Table 1. In this calculation matrix effects are ignored as are mean-free-path differences. The compositions of the surfaces after annealing the sample at various temperatures and calculated using these same sets of sensitivity factors are shown in Table 2.

ISS is a powerful surface characterization technique which provides compositional information concerning the outermost atomic layer. This technique is particularly useful when performed in conjunction with XPS since XPS probes as far as 60 Å beneath the surface. The ISS spectrum taken from the as-entered sample is shown in Figure 5a. The primary feature is due to Ag while small C and O features are apparent also. A previous study[6] has demonstrated that the cross section of Ag is more than 20 times greater than that of O in ISS. This result and the ISS data shown in Figure 5a indicate that the outermost layer of the as-entered sample consists primarily of C and O. According to XPS, hydrocarbon contamination is present which most likely resides at the surface since it was absorbed during air exposure. This contributes to the C and O feature present in this ISS spectrum.

The high-resolution XPS spectra shown in Figures 1−4 and labeled (b) were taken after a 155 °C anneal treatment. The Ag 3d features are shifted slightly to a higher BE due to the formation of some metallic Ag and $Ag_2O$ during this anneal. Furthermore, the fwhm of the Ag $3d_{5/2}$ peak is decreased from 1.5 to 1.4, indicating a shift away from the $Ag_2CO_3$ state at lower BE. The O 1s peak (Figure 2b) remains unshifted in BE, but its width is reduced. It also exhibits a broad and flat shoulder on the low-BE side due to the presence of chemisorbed O, AgO, and $Ag_2O$. The chemisorbed O is often present after $Ag_2CO_3$ or Ag oxides decompose to form Ag metal.[1,2] The C 1s spectrum (Figure 3b) contains no contribution from hydrocarbon contamination, and the primary C 1s feature is still due to $Ag_2CO_3$. The Ag(*MNN*) spectrum is very different after the 155 °C anneal (Figure 4b). The $Ag_2CO_3$ feature is significantly decreased, the feature due to metallic Ag is increased, and some $Ag_2O$ and AgO are present. These observations are consistent with the XPS core-level data, but they are more readily apparent in the AES data. The ISS spectrum obtained from the $Ag_2CO_3$ powder sample after the 155 °C anneal is shown in Figure 5b. The C and O peaks are essentially eliminated, indicating that most of the C and O that was present at the outermost atomic layer of the untreated $Ag_2CO_3$ powder is removed by this heat treatment, leaving nearly all Ag in the outermost atomic layer.

Upon heating this sample at 170 °C, some of the $Ag_2CO_3$ decomposes, resulting in a rapid increase of the UHV chamber pressure. The XPS Ag 3d spectrum obtained from the sample after this anneal is shown in Figure 1c. Again, the peak maximum is shifted to slightly higher BE due to formation of more metallic Ag. The fwhm is increased from 1.4 to 1.5 due to the formation of metallic Ag and Ag oxides (both AgO and $Ag_2O$). The XPS O 1s spectrum obtained after the 170 °C anneal is shown in Figure 2c. Significant changes in the chemical nature of the oxygen occur between 155 and 170 °C. The predominant feature due to O in $Ag_2CO_3$ is further reduced in intensity by decomposition of the carbonate to $Ag_2O$, AgO, and Ag metal. Increased O features are also apparent for $Ag_2O$ and AgO. Structure due to two forms of O associated with Ag metal is apparent as well. The feature due to chemisorbed O at 528.3 eV is increased in intensity, and a shoulder due to subsurface (or dissolved) O is apparent at a BE of 531.4 eV. These decomposition reactions do not occur instantaneously at the conditions predicted by equilibrium thermodynamics. They are activated so they occur at rates that are strongly dependent upon temperature. If this sample were held at 170 °C for a

**TABLE 1: Sensitivity Factors and Calculated Compositions for the As-Entered $Ag_2CO_3$**

| species | PHI (ref 35) sensitivity factors | atomic concentration | PHI (ref 36) sensitivity factors | atomic concentration | calculated sensitivity factors | atomic concentration |
|---|---|---|---|---|---|---|
| Ag as $Ag_2CO_3$ | 2.25 | 34.6 | 5.987 | 19.9 | 3.44 | 28.1 |
| Ag metal | 2.25 | 0.8 | 5.987 | 0.4 | 3.44 | 2.1 |
| O as $Ag_2CO_3$ | 0.63 | 38.3 | 0.71 | 51.9 | 0.711 | 42.5 |
| C as $Ag_2CO_3$ | 0.205 | 13.3 | 0.296 | 14.0 | 0.24 | 13.8 |
| C contamination | 0.205 | 13.0 | 0.296 | 13.8 | 0.24 | 13.5 |

**TABLE 2: Calculated Compositions for the Thermally Treated $Ag_2CO_3$ Sample**

| | PHI (ref 35) | | | PHI (ref 36) | | | calculated | | |
|---|---|---|---|---|---|---|---|---|---|
| *T* (°C) | Ag | O | C | Ag | O | C | Ag | O | C |
| 155 | 52.5 | 36.6 | 10.9 | 33.0 | 54.3 | 12.7 | 45.1 | 42.6 | 12.3 |
| 170 | 69.4 | 23.0 | 7.6 | 50.4 | 39.4 | 10.2 | 62.8 | 28.2 | 9.0 |
| 205 | 71.7 | 23.3 | 5.0 | 52.6 | 40.4 | 7.0 | 65.2 | 28.7 | 6.1 |
| 340 | 82.6 | 17.4 | 0 | 66.7 | 33.3 | 0 | 77.7 | 22.3 | 0 |
| 430 | 93.3 | 6.7 | 0 | 85.6 | 14.4 | 0 | 91.2 | 8.8 | 0 |

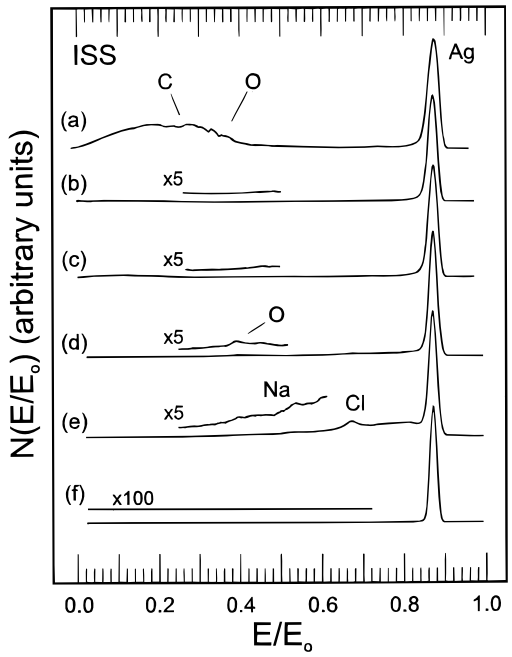


**Figure 5.** ISS spectra obtained from the as-received $Ag_2CO_3$ powder after (a) insertion into the UHV chamber, (b) a 155 °C anneal for $^1/_2$ h, (c) a 170 °C anneal for $^1/_2$ h, (d) a 205 °C anneal for $^1/_2$ h, (e) a 340 °C anneal for $^1/_2$ h, and (f) a 430 °C anneal for $^1/_2$ h.

longer period, more of the $Ag_2CO_3$ would have decomposed. The C 1s feature obtained from this surface is shown in Figure 3c. The peak due to carbonate is significantly reduced in size.

The XPS Ag *MNN* spectrum taken after the 170 °C anneal is shown in Figure 4c. The $Ag_2CO_3$ feature is decreased further, and the features due to Ag metal and AgO are more prominent. Changes in the amount of Ag can also be observed by following the behavior of the Ag Auger peak at 895.0 eV. The feature due to $Ag_2O$ is also less prominent, indicating decomposition of this species to Ag metal. The ISS spectrum shown in Figure 5c indicates that the outermost atomic layer still consists primarily of Ag.

The sample was next heated to 205 °C for $^1/_2$ h, and the high-resolution XPS spectra obtained after this treatment are shown in Figures 1d−4d. The Ag $3d_{5/2}$ peak now has a BE of 367.2 eV, which corresponds mostly to AgO, some $Ag_2O$, and a small amount of $Ag_2CO_3$. The O 1s spectrum shown in Figure 2d exhibits a smaller $Ag_2CO_3$ feature and indicates that more O is now bound to Ag as AgO. However, structures due to chemisorbed and subsurface O species are also observable in this spectrum. The C 1s feature due to carbonate (Figure 3d) is diminished nearly to the noise level. The Ag *MNN* feature (Figure 4d) also contains a larger contribution from AgO in the near-surface region, and again the contribution from the carbonate species is further diminished. The ISS spectrum obtained from the 205 °C annealed sample is shown in Figure 5d. The intensity of the O peak actually increases during the 205 °C anneal, indicating that the outermost atomic layer contains more oxygen. This implies that diffusion of bulk oxygen to the outermost surface layer occurs more rapidly at this temperature than desorption which results in an increase of the surface O concentration.

The Ag 3d XPS spectrum obtained from the sample after the 340 °C anneal (Figure 1e) indicates that the Ag in the near-surface region is now present primarily as $Ag_2O$. The Ag $3d_{5/2}$ feature has a reduced fwhm of 1.3 eV denoting a decrease in the amounts of different chemical states present. The corresponding O 1s spectrum (Figure 2e) indicates that the near-surface oxygen is primarily bound as $Ag_2O$ although small amounts of AgO, chemisorbed O, and subsurface O are evident as well. The Ag *MNN* peaks, shown in Figure 4e, are more well-defined after this thermal treatment which is consistent with the presence of fewer Ag chemical states. No features are discernible in the C 1s XPS spectrum obtained after this anneal so it is not shown. The ISS spectrum collected after the 340 °C anneal in the UHV chamber for $^1/_2$ h is shown in Figure 5e. Oxygen is still present at the outermost layer with little change in the intensity of its feature. A Cl peak and a Na peak due to bulk contamination are now present which are not previously observable. Apparently these species migrate to the outermost atomic layer during this treatment.

A final anneal treatment of 430 °C for $^1/_2$ h was performed, and the high-resolution XPS spectra obtained after this treatment are shown in Figures 1f, 2f, and 4f. The Ag 3d and Ag *MNN* spectral features indicate that the $Ag_2CO_3$ and Ag oxides subsequently formed are now completely decomposed to Ag metal. A small amount of subsurface oxygen is present according to the O 1s spectrum (Figure 2f). The presence of subsurface hydroxyl groups tends to broaden this feature on the high-BE side.[1,2] Previously obtained data using angle-resolved Auger electron spectroscopy (ARAES) indicates that subsurface O is very persistent in the Ag metal matrix and remains even after a 30 min, 1 keV $Ar^+$ sputter and 35 min, 250 °C anneal cycle.[6] An ISS spectrum taken from the sample after the 430 °C annealing treatment is shown in Figure 5f. The Ag peak is the only feature observable even after a 100× magnification of the signal.

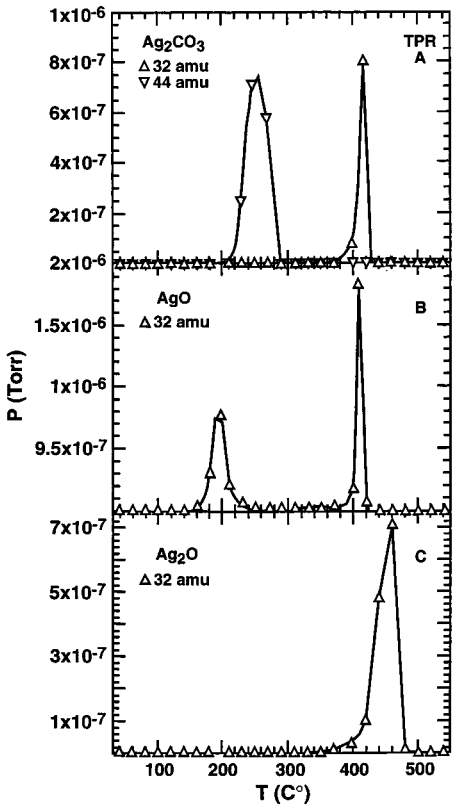


**Figure 6.** TPR data obtained from (A) $Ag_2CO_3$ powder, (B) AgO powder, and (C) $Ag_2O$ powder.

TPR data obtained from $Ag_2CO_3$, AgO, and $Ag_2O$ powders are shown in Figure 6, A, B, and C, respectively. The primary desorption peaks from $Ag_2CO_3$ consist of $CO_2$ with a maximum at about 260 °C and $O_2$ with a maximum at about 420 °C. No features due to $H_2$ or $H_2O$ were obtained. The primary desorption peaks from AgO consist of two $O_2$ peaks of approximately equal areas and peak maxima at about 190 and 410 °C. These results are in complete agreement with the previous thermal decomposition study of AgO[1] in which it was found that AgO first decomposes to $Ag_2O$ and then Ag metal at these same temperatures using XPS. Very small peaks due to $H_2O$ and $CO_2$ also occur at about 190 °C (not shown). These are about 1/20th the size of the $O_2$ peak. Another small $CO_2$ peak is present at about 360 °C, but no $H_2O$ peak is present at this temperature. Possibly, the lower temperature peak is due to decomposition of bicarbonate and the higher temperature peak is due to decomposition of carbonate, but neither of these peaks corresponds to the decomposition temperature of bulk $Ag_2CO_3$. However, $Ag_2O$ exhibits one $O_2$ desorption peak with a peak maximum of 460 °C and complete decomposition at 490 °C. Similar small $CO_2$ adsorption peaks are apparent as found for AgO, but a water peak is not observed. Again, these results are in complete agreement with the previous thermal decomposition study of $Ag_2O$.[2] In the thermal decomposition of both AgO and $Ag_2O$, there is a reaction due to $Ag_2O$ forming Ag metal and $O_2$. In the case of AgO decomposition, this reaction occurs with a peak maximum about 40 °C lower than that of $Ag_2O$. This is probably due to formation of a $Ag_2O$ defect structure after decomposition of AgO. This defect structure apparently has a significantly lower decomposition temperature than well-ordered $Ag_2O$. In the decomposition of $Ag_2CO_3$, this step occurs at 420 °C ,which is only 10 °C higher than the same step in AgO decomposition. When $Ag_2CO_3$ decomposes and releases $CO_2$ to form $Ag_2O$, this $Ag_2O$ structure is defect-laden and has a decomposition structure that is similar to the defect-laden $Ag_2O$ structure formed during thermal decomposition of AgO. The fact that the TPR features do not have high-temperature tails indicates that the gas transport properties through the pressed pellet do not influence the TPR data. So little water is present that it also is not believed to have an influence on the decomposition behavior.

XPS, ISS, and TPR examine very different regions of the sample. For the most part TPR is a bulk technique with regard to the predominant features in this study, but it is also surface sensitive in that surface species yield small peaks such as the $CO_2$ peaks produced in the AgO and $Ag_2O$ TPR. XPS and ISS also probe different regions of the surface. XPS typically probes 40−60 Å beneath the surface, and ISS probes only the outermost atomic layer so compositions determined by XPS and ISS usually differ for complex samples. Furthermore, the bulk composition is usually quite different than the surface composition, and depth profiling using ion sputtering can provide information about this difference. Nevertheless, there is an interesting connection between the surface techniques and TPR in these decomposition studies in that all vapor species produced by decomposition in the bulk must pass through the surface region and desorb. Generally, there is a remarkable correspondence between the XPS and TPR data. The TPR experiments yield well-defined features that do not shift in temperature with heating rate or even the use of stepwise heating,[1,2] indicating that the decomposition temperatures are determined by the heights of activation barriers rather than kinetic considerations. Thermodynamic equilibrium calculations predict that $Ag_2CO_3$, $Ag_2O$, and AgO should decompose at much lower temperatures than they actually do because these calculations do not take activation barriers into account.

## Summary

An as-received $Ag_2CO_3$ powder sample was examined using XPS and ISS before and during its thermal decomposition under UHV. The near-surface region of the as-entered powder consists primarily of $Ag_2CO_3$ although some alcohol and hydrocarbon contamination is present also. The ISS data indicate that these contaminants reside at the surface. After annealing the sample at 155 °C for $^1/_2$ h in a vacuum, some of the $Ag_2CO_3$ is decomposed to Ag metal and oxides, and the amount of hydrocarbon and alcohol contamination is decreased. Between 155 and 170 °C more $Ag_2CO_3$ decomposes to Ag oxides and metal. After the 205 °C anneal no C is present in the near-surface region, and an enrichment of O at the outermost surface layer is observed. The Ag oxides undergo thermal decomposition between 340 and 430 °C to Ag metal, and a small amount of subsurface oxygen persists in the near-surface region after this anneal. TPR data are consistent with the XPS data. The $Ag_2CO_3$ decomposes to $CO_2$ and $Ag_2O$ at about 260 °C, and then the $Ag_2O$ decomposes to Ag metal and $O_2$ at about 420 °C. The decomposition of this $Ag_2O$ occurs at the same temperature as $Ag_2O$ formed by thermal decomposition of AgO but about 40 °C lower than bulk $Ag_2O$ powder. This fact suggests that the $Ag_2O$ formed by thermal decomposition of $Ag_2CO_3$ and AgO consists of a defect-laden structure that decomposes more readily than well-ordered $Ag_2O$.

**Acknowledgment.** Financial support for this research was obtained from the National Science Foundation through Grant CTS-9122575.

## References and Notes

(1) Weaver, J. F.; Hoflund, G. B. *J. Phys. Chem.* **1994**, *98*, 8519.
(2) Weaver, J. F.; Hoflund, G. B. *Chem. Mater.* **1994**, *6*, 1693.

(3) Hoflund, G. B.; Weaver, J. F.; Epling, W. S. *Surf. Sci. Spectra* **1996**, *3*, 157.
(4) Hoflund, G. B.; Weaver, J. F.; Epling, W. S. *Surf. Sci. Spectra* **1996**, *3*, 163.
(5) Hoflund, G. B.; Weaver, J. F.; Epling, W. S. *Surf. Sci. Spectra* **1996**, *3*, 151.
(6) Davidson, M. R.; Hoflund, G. B.; Outlaw, R. A. *J. Vac. Sci. Technol. A* **1991**, *9*, 1344.
(7) Corallo, G. R.; Hoflund, G. B.; Outlaw, R. A. *Surf. Interface Anal.* **1988**, *12*, 185.
(8) Outlaw, R. A.; Sankaran, S. N.; Hoflund, G. B.; Davidson, M. R. *J. Vac. Sci. Technol. A* **1988**, *6*, 2280.
(9) Outlaw, R. A.; Hoflund, G. B.; Davidson, M. R. *J. Vac. Sci. Technol. A* **1989**, *7*, 2087.
(10) Lee, W. S.; Outlaw, R. A.; Hoflund, G. B.; Davidson, M. R. *Appl. Surf. Sci*. **1991**, *47*, 91.
(11) Outlaw, R. A.; Wu, D.; Davidson, M. R.; Hoflund, G. B. *J. Vac. Sci. Technol. A* **1992**, *10*, 1497.
(12) Davidson, M. R.; Hoflund, G. B.; Outlaw, R. A. *Surf. Sci*. **1993**, *28*, 111.
(13) Schön, G. *Acta Chem. Scand*. **1973**, *27*, 2623.
(14) Hammond, J. S.; Gaarenstroom, S. W.; Winograd, N. *Anal. Chem*. **1975**, *47*, 2193.
(15) Gaarenstroom, S. W.; Winograd, N. *J. Phys. Chem*. **1977**, *67*, 15.
(16) Rehren, C.; Isaac, G.; Schlögl, R.; Ertl, G. *Catal. Lett*. **1991**, *11*, 253.
(17) Campbell, C. T. *Surf. Sci*. **1985**, *157*, 43.
(18) Bowker, M.; Barteau, M. A.; Madix, R. J. *Surf. Sci*. **1980**, *92*, 528.
(19) Lefort, T. E. (to Societe Francaise de Catalyse Generalisee) Fr. Pat. 729,952.
(20) Nielsen, R. P.; LaRochelle, J. H. U.S. Patent 3 962 136, 1976 and U.S. Patent 4 012 426, 1977.
(21) Berty, J. M. In *Applied Industrial Catalysis*; Leach, B. E., Ed.; Academic Press: New York, 1983−1984; Vol. 1, p 207.
(22) Satterfield, C. N. *Heterogeneous Catalysis in Industrial Practice*, 2nd ed.; McGraw-Hill: New York, 1991.
(23) Van Santen, R. A.; Kuipers, H. P. C. E. *Adv. Catal*. **1987**, *35*, 265.
(24) Boronin, A. I.; Bukhtiyarov, V. I.; Vishnevskii, A. L.; Boreskov, G. K.; Savchenko, V. I. *Surf. Sci*. **1988**, *201*, 195.
(25) Minahan, D. M.; Hoflund, G. B. *J. Catal.* **1996**, *158*, 109.
(26) Hoflund, G. B.; Minahan, D. M. *J. Catal*. **1996**, *162*, 48.
(27) Minahan, D. M.; Hoflund, G. B.; Epling, W. S.; Schoenfeld, D. W. *J. Catal*. **1997**, *168*, 393.
(28) Epling, W. S.; Hoflund, G. B.; Minahan, D. M. *J. Catal.* **1997**, *171*, 490.
(29) Jun, Y.; Jingfa, D.; Xiaohong, Y.; Shi, Z. *Appl. Catal. A* **1992**, *92*, 73.
(30) Gorcharova, S. N.; Paukshtis, E. A.; Bal'zhinimaev, B. S. *Appl. Catal. A* **1995**, *126*, 67.
(31) Gilbert, R. E.; Cox, D. F.; Hoflund, G. B. *Rev. Sci. Instrum*. **1982**, *53*, 1281.
(32) Epling, W. S.; Hoflund, G. B. *Surf. Sci. Spectra* **1998**, *00*, 00.
(33) Campbell, C. T.; Paffett, M. T. *Surf. Sci.* **1984**, *143*, 517.
(34) Campbell, C. T. *Surf. Sci.* **1985**, *157*, 43.
(35) Wagner, C. D.; Riggs, W. M.; Davis, L. E.; Moulder, J. F.; Muilenberg, G. E. *Handbook of X-ray Photoelectron Spectroscopy, Physical Electronics*; Perkin-Elmer: Eden Prairie, MN, 1979.
(36) Moulder, J. F.; Stickle, W. F.; Sobol, P. E.; Bomben, K. D. In *Handbook of X-ray Photoelectron Spectroscopy*; Chastain, J., Ed.; Perkin-Elmer: Eden Prairie, MN, 1992.